Cell Reports Medicine, Volume *4*

Supplemental information

Proteomics separates adult-type diffuse high-grade gliomas in metabolic subgroups independent of 1p/19q codeletion and across IDH mutational status

Jakob Maximilian Bader, Nikolaus Deigendesch, Martin Misch, Matthias Mann, Arend Koch, and Felix Meissner

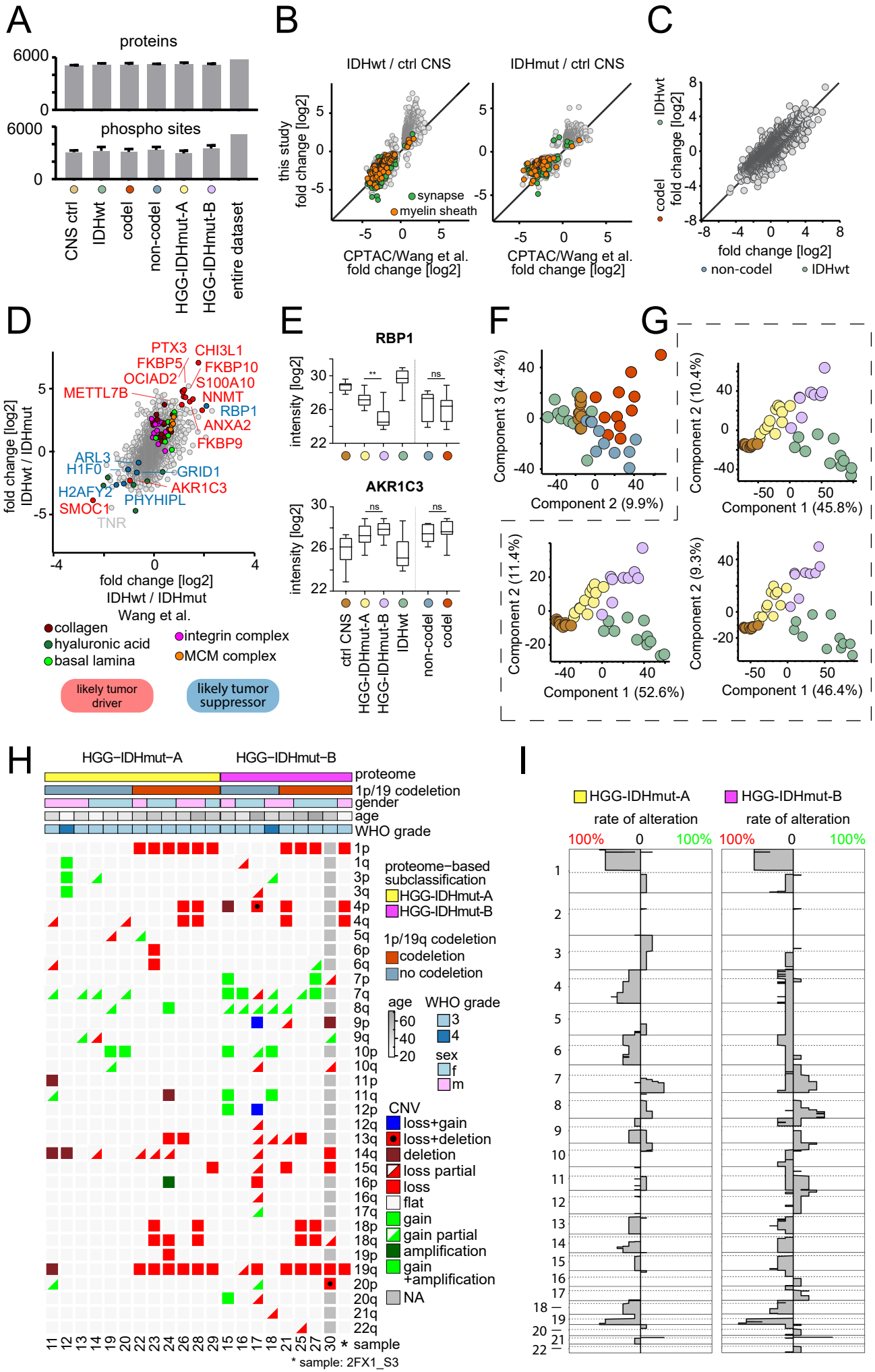
A
proteins
6000
0
phospho sites
6000
0
CNS ctrl
IDHwt
codel
non-codel
HGG-IDHmut-A
HGG-IDHmut-B
entire dataset
B
IDHwt / ctrl CNS
IDHmut / ctrl CNS
this study fold change [log2]
synapse
myelin sheath
CPTAC/Wang et al. fold change [log2]
C
IDHwt
codel
fold change [log2]
non-codel
IDHwt
D
PTX3
CHI3L1
FKBP5
FKBP10
OCIAD2
S100A10
METTL7B
NNMT
RBP1
ANXA2
FKBP9
ARL3
H1F0
GRID1
H2AFY2
AKR1C3
PHYHIPL
SMOC1
TNR
fold change [log2] IDHwt / IDHmut
fold change [log2] IDHwt / IDHmut Wang et al.
collagen
hyaluronic acid
basal lamina
integrin complex
MCM complex
likely tumor driver
likely tumor suppressor
E
RBP1
AKR1C3
intensity [log2]
ctrl CNS
HGG-IDHmut-A
HGG-IDHmut-B
IDHwt
non-codel
codel
F
Component 3 (4.4%)
Component 2 (9.9%)
Component 2 (10.4%)
Component 1 (45.8%)
Component 2 (11.4%)
Component 1 (52.6%)
Component 2 (9.3%)
Component 1 (46.4%)
G
H
HGG−IDHmut−A
HGG−IDHmut−B
proteome
1p/19 codeletion
gender
age
WHO grade
proteome−based subclassification
HGG-IDHmut-A
HGG-IDHmut-B
1p/19q codeletion
codeletion
no codeletion
age
WHO grade
sex
CNV
loss+gain
loss+deletion
deletion
loss partial
loss
flat
gain
gain partial
amplification
gain +amplification
NA
* sample
* sample: 2FX1_S3
I
HGG-IDHmut-A
HGG-IDHmut-B
rate of alteration
100%
0
100%

Figure S1. Overall dataset, separation glioma subgroups and comparison to CPTAC/Wang et al. dataset. Related to Figure 1.

A) Number of quantified proteins and high-confidence class I (localization probability > 0.75) phosphor-sites in filtered dataset. Samples, n=10 (ctrl CNS), n=12 (HGG-IDHmut-A), n=9 (HGG-IDHmut-B), n=11 (IDHwt), n=11 (codel), n=10 (non-codel).

B) Comparison of CPTAC/Wang et al. glioma proteome data to our glioma dataset. Specifically, comparison of IDHwt to ctrl CNS protein fold changes [log2] (left) and IDHmut to ctrl CNS protein fold changes [log2] right. Entities nmf1, nmf2, nmf3 in CPTAC dataset are IDHwt. Only proteins significantly regulated (q < 5%) in at least one dataset included: 2732 (IDHwt vs ctrl CNS) and 1351 (IDHmut vs ctrl CNS). Consistency of regulation: 99% concordance and Pearson r = 0.92 (IDHwt vs ctrl CNS) and 98% concordance and Pearson r = 0.91 (IDHmut vs ctrl CNS). Samples, this study: n=10 (ctrl CNS), n=11 (IDHwt), Wang et al.: n=10 (ctrl CNS), n=91 (IDHwt).

C) IDHwt/IDHmut proteome differences depending on 1p/19q-codeletion status of IDHmut. Samples as in A.

D) Comparison of IDHwt/IDHmut differences between datasets of this study (y axis) and CPTAC (x axis). Entities nmf1, nmf2, nmf3 in CPTAC/Wang et al. dataset are IDHwt. All proteins overlapping in both datasets (5241) shown, Pearson r = 0.57. Filtering for proteins significantly regulated (q < 5%) in both datasets, increases correlation to Pearson r = 0.89 (701 proteins). Outlier proteins and proteins belonging to enriched annotation terms of interest as in Fig. 1E highlighted. Samples, this study: n=21 (IDHmut), n=10 (IDHwt), CPTAC/Wang: n=6 (IDHmut), n=91 (IDHwt).

E) Abundances of RBP1 and AKR1C3 across sample groups of this study. Samples as in A.

F) Separation of codeleted and non-codeleted IDH-mutant samples in the combined second and third components of the principal component analysis of the glioma proteome. Green IDHwt, brown ctrl CNS, red 1p/19q-codeleted IDH-mutant, blue non-1p/19q-codeleted samples. Samples as in A.

G) Equivalence of the HGG-IDHmut-A / HGG-IDHmut-B subgroup clustering in differently filtered datasets. PCA analysis of dataset comprising ANOVA-significant (q < 5%) proteins (top right, 3749 proteins), dataset comprising proteins quantified in all 42 samples without missing values (bottom left, 2625 proteins), and dataset comprising the top 25% most variable proteins with highest CVs across all 42 samples (bottom right, 1439 proteins). Samples as in A.

H) CNV profiles across samples. Samples as in A.

I) CNV load plots as averages within the groups of HGG-IDHmut-A and HGG-IDHmut-B. Amplifications highlighted as alterations in green to the right, deletions as alterations in red to the left. Samples as in A.

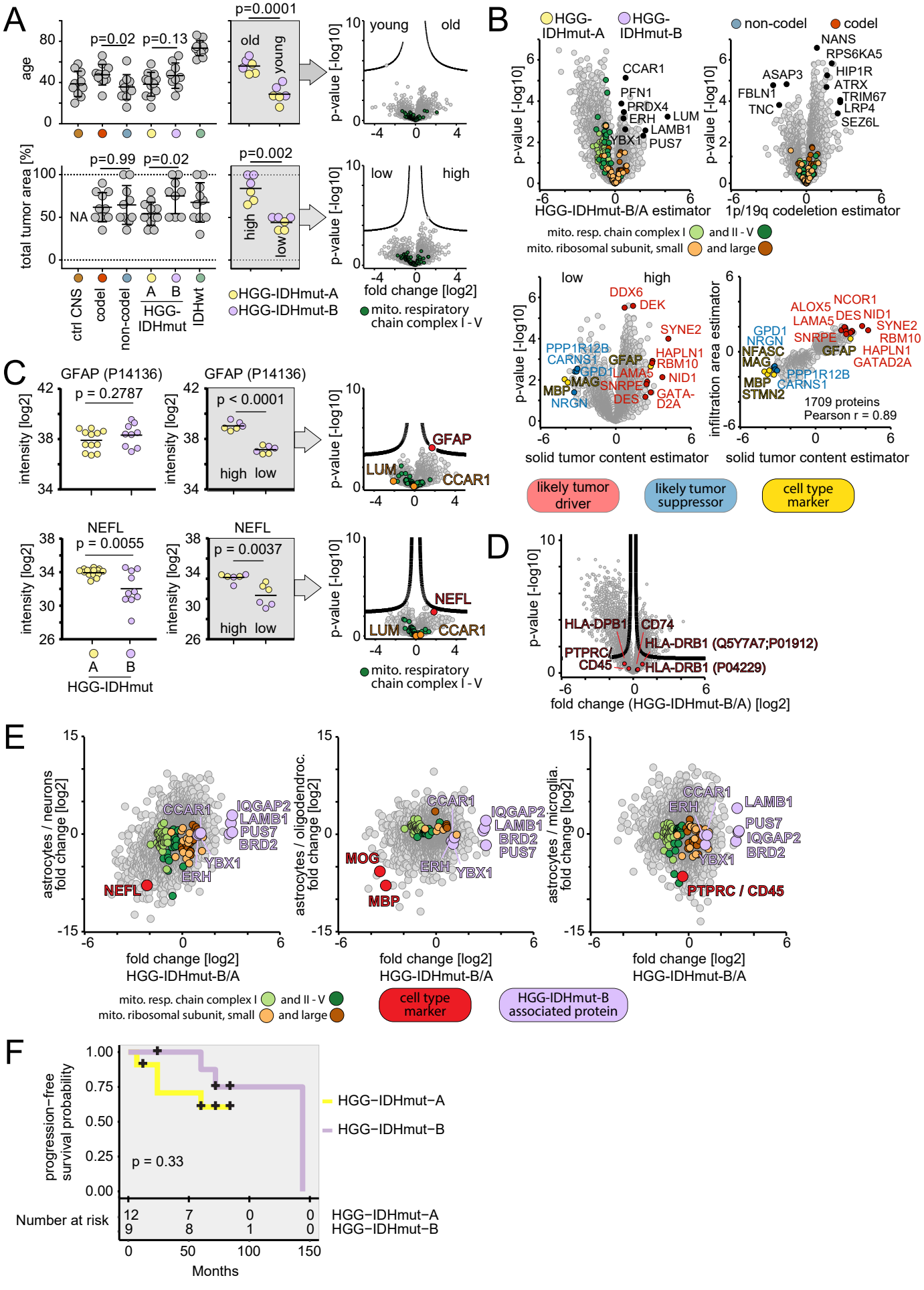
A
age
p=0.02
p=0.13
p=0.0001
old
young
p-value [-log10]
young
old
total tumor area [%]
p=0.99
p=0.02
p=0.002
high
low
NA
fold change [log2]
ctrl CNS
codel
non-codel
A
B
HGG-IDHmut
IDHwt
HGG-IDHmut-A
HGG-IDHmut-B
mito. respiratory chain complex I - V
B
HGG-IDHmut-A
HGG-IDHmut-B
CCAR1
PFN1
PRDX4
ERH
LUM
LAMB1
YBX1
PUS7
HGG-IDHmut-B/A estimator
non-codel
codel
NANS
RPS6KA5
HIP1R
ATRX
TRIM67
LRP4
SEZ6L
ASAP3
FBLN1
TNC
1p/19q codeletion estimator
mito. resp. chain complex I and II - V
mito. ribosomal subunit, small and large
low
high
DDX6
DEK
SYNE2
PPP1R12B
CARNS1
GFAP
HAPLN1
RBM10
GPD1
LAMA5
NID1
MAG
SNRPE
MBP
NRGN
DES
GATA-D2A
solid tumor content estimator
ALOX5
NCOR1
LAMA5
DES
NID1
SYNE2
GPD1
NRGN
SNRPE
RBM10
NFASC
GFAP
HAPLN1
MAG
GATAD2A
PPP1R12B
CARNS1
MBP
STMN2
infiltration area estimator
1709 proteins
Pearson r = 0.89
likely tumor driver
likely tumor suppressor
cell type marker
C
GFAP (P14136)
p = 0.2787
p < 0.0001
intensity [log2]
high low
GFAP
LUM
CCAR1
NEFL
p = 0.0055
p = 0.0037
A
B
HGG-IDHmut
mito. respiratory chain complex I - V
D
p-value [-log10]
HLA-DPB1
CD74
PTPRC/ CD45
HLA-DRB1 (Q5Y7A7;P01912)
HLA-DRB1 (P04229)
fold change (HGG-IDHmut-B/A) [log2]
E
astrocytes / neurons fold change [log2]
astrocytes / oligodendroc. fold change [log2]
astrocytes / microglia. fold change [log2]
CCAR1
IQGAP2
LAMB1
PUS7
BRD2
YBX1
ERH
NEFL
MOG
MBP
PTPRC / CD45
fold change [log2] HGG-IDHmut-B/A
mito. resp. chain complex I and II - V
mito. ribosomal subunit, small and large
cell type marker
HGG-IDHmut-B associated protein
F
progression-free survival probability
p = 0.33
HGG−IDHmut−A
HGG−IDHmut−B
Number at risk
12 7 0 0
9 8 1 0
Months

Figure S2. Analysis of HGG-IDHmut-A/B association with patient demographics, survival and tumor content. Related to Figure 1.

Upon identification of the proteome-based classification, we aimed to link this classification to patient's demographic data or histological correlates.

- **A)** Influence of patient age (top row) and tumor content (bottom row) on HGG-IDHmut-A/B separation. Left: Distribution of values (top: patient age at diagnosis, bottom: area % of sample that is tumor according to histopathological assessment) across sample groups of this study. Samples, n=10 (ctrl CNS), n=12 (HGG-IDHmut-A), n=9 (HGG-IDHmut-B), n=11 (IDHwt), n=11 (codel), n=10 (non-codel). Center: Stratification of control groups (n=6 in each group) for age (top) and tumor content (bottom), balanced for HGG-IDHmut-A and B composition, respectively. Right: Proteome differences between stratified control groups, mitochondrial respiratory chain proteins highlighted. A neuropathologist did not identify discerning histomorphological features, but estimated the fractions of the tissue section occupied by the solid tumor, the tumor infiltration zone, and the reactive CNS tissue for further analysis. Moderately higher total tumor area (solid + infiltration) in HGG-IDHmut-B comparted to A. However, no significant proteome differences between groups of samples stratified into 'high tumor area' and a 'low tumor area' for total tumor area, (and likewise for solid or infiltration area, not shown).
- **B)** Linkage of differential tumor content to independent cancer drivers but not the HGG-IDHmut-A/B separation. Linear regression model predicting protein intensity based on variables HGG-IDHmut-A/B status, 1p/19q codeletion status, solid tumor content, tumor infiltration area. Regression results showing estimators (x axis) for HGG-IDHmut-A/B status (top left), 1p/19q codeletion status (top right), solid tumor content (bottom left), and their significance (y axis), respectively. Correlation of estimators for solid tumor area and tumor infiltration area (bottom right) for proteins significant ($p <$ 5%) in at least one tumor area dimension. Proteins of interest highlighted including mitochondrial proteins (top row) and tumor suppressor, oncoproteins, and cell type markers (bottom row). Samples, n=12 (HGG-IDHmut-A), n=9 (HGG-IDHmut-B), n=11 (codel), n=10 (non-codel). Main features of HGG-IDHmut-A/B separation (mito. resp. chain complex signature, outlier proteins) confirmed, and 1p/19q codel-associated protein regulation preserved and statistically more significant, after correction for covariates by regression model. Outlier proteins associated with solid or infiltration tumor area distinct to the proteins linked to either subgrouping (HGG-IDHmut-A/B or 1p/19q status) but protein association with the two tumor area parameters highly correlated. Many high tumor content-associated proteins previously implicated as oncogenes, predominantly in other cancer types, including NID1, SYNE2, DEK, DDX6, DES, GATAD2A, SNRPE, ALOX5, HAPLN1, LAMA5, NCOR1, and RBM10[145-157]. Conversely, low tumor content proteins comprising functional CNS proteins such as myelin (MBP, MAG) and neuronal proteins (NFASC, STMN2), and tumor suppressors (NRGN, CARNS1, GPD1[158-160]).
- C) Relationship of HGG-IDHmut-A/B separation and differential content of astrocyte and neuron content. Sample numbers as in B. Left: Distribution of values (top: GFAP intensity, bottom: NEFL intensity) across sample groups of this study. Center: Stratification of control groups (n=6 in each group) for GFAP intensity (top) and NEFL intensity (bottom) balanced for HGG-IDHmut-A and B composition, balanced for HGG-IDHmut-A and B composition, respectively. Right: Proteome differences between stratified control groups, mitochondrial respiratory chain proteins and proteins of interest highlighted. No significant proteome alterations or differences of mitochondrial respiratory chain proteins as in HGG-IDHmut-A/HGG-IDHmut-B comparison in these stratifications.
- D) Apparent non-regulation of microglia-associated proteins between HGG-IDHmut-A (n=12) and B (n=9) proteome.
- E) Comparison of proteome differences between HGG-IDHmut-A / B sample groups and differences between isolated astrocytes and neurons (left), astrocytes and oligodendrocytes (center), and astrocytes and microglia (right) accessible for mouse[144]. No correlation of mitochondrial protein abundance differences between the HGG-IDHmut-A/B subtypes with the abundance differences between isolated brain cell types. Proteins with q-value of 5% or lower in at least one of the two dimensions each (cell types, glioma subtypes) included. Neuronal (NEFL), oligodendroglial (MOG, MBP) and microglial marker proteins (PTPRC/CD45) labelled in red. Outlier proteins associated with HGG-IDHmut-B labelled in pink. Mitochondrial respiratory chain proteins green and mitochondrial ribosomal proteins brown. Respiratory chain complex V refers to ATP synthase. Pearson correlation coefficients for all

proteins, left: r = 0.41, center: r = 0.09, right: r = -0.12 and for labelled mitochondrial proteins, left: r = -0.04, center: r = -0.03, right: r = -0.08. Samples, n= 12 (HGG-IDHmut-A), n=9 (HGG-IDHmut-B), n=3 (astrocytes), n=3 (oligodendrocytes DIV4), n=3 (neurons DIV15), n=3 (adult microglia).

F) Progression-free survival of HGG-IDHmut-A (n=12) and HGG-IDHmut-B (n=9).

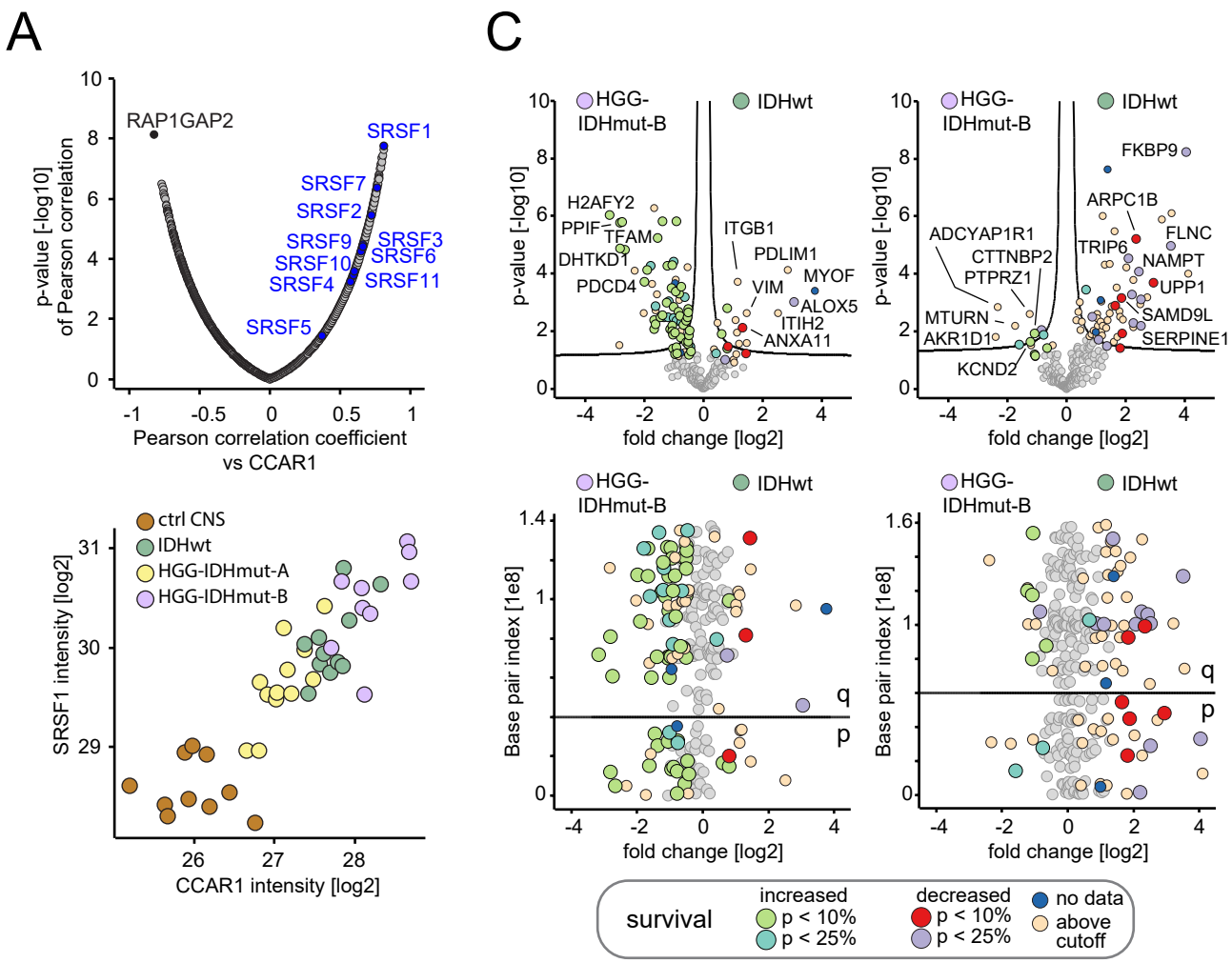
A
RAP1GAP2
SRSF1
SRSF7
SRSF2
SRSF9
SRSF3
SRSF10
SRSF6
SRSF4
SRSF11
SRSF5
p-value [-log10] of Pearson correlation
Pearson correlation coefficient vs CCAR1
ctrl CNS
IDHwt
HGG-IDHmut-A
HGG-IDHmut-B
SRSF1 intensity [log2]
CCAR1 intensity [log2]
C
HGG-IDHmut-B
IDHwt
H2AFY2
PPIF
TFAM
DHTKD1
PDCD4
ITGB1
PDLIM1
MYOF
VIM
ALOX5
ITIH2
ANXA11
FKBP9
ARPC1B
ADCYAP1R1
FLNC
TRIP6
CTTNBP2
NAMPT
PTPRZ1
UPP1
MTURN
SAMD9L
AKR1D1
SERPINE1
KCND2
p-value [-log10]
fold change [log2]
Base pair index [1e8]
q
p
survival
increased
p < 10%
p < 25%
decreased
p < 10%
p < 25%
no data
above cutoff
B
nuclear telomere cap complex
G-rich strand telomeric DNA binding
telomerase RNA binding
telomere maintenance via telomerase
19q arm
1p arm
rank
annotation enrichment score in Pearson coeffiecient for ATRX-correlation
GGH
CTSD
GMPS
NANS
RPA1
XRCC6
TERF2
RAD50
HNRNPU
TERF2IP
GAR1
XRCC5
HSP90AB1
HNRNPA2B1
MRE11A
SNRPB
DKC1
HNRNPC
DHX36
HNRNPA1
NHP2
SNRPD3
HSP90AA1
HNRNPC
PTGES3
RPA2
PARN
EXOSC10
TNKS1BP1
p-value [-log10] of Pearson correlation
Pearson correlation coefficient vs ATRX
D
chromosome arm 1p
chromosome arm 19q
non-codel
codel
LRRC40
MANEAL
PKN2
ATPIF1
p-value [-log10]
fold change [log2]
Base pair index [1e8]
p
q

Figure S3: CCAR1 and ATRX correlation analysis, survival association of regulated chr. 7, chr. 10, and 1p/19q proteins. Related to Figure 2.

A) CCAR1 correlation analysis. Top: Proteins correlating to CCAR1 across all 32 tumor samples. Bottom: Abundances of CCAR1 and SRSF1 across all samples of dataset. Pearson coefficient r = 0.89. Sample groups color-coded, brown control CNS, green IDHwt, yellow HGG-IDHmut-A, pink HGG-IDHmut-B.

B) ATRX correlation analysis. Top: Annotations enriched in proteins with extreme (high/low) Pearson correlation coefficients vs ATRX according to Perseus 1D annotation enrichment. IDHmut tumors (n=21) included. 1p/19q affiliation of proteins treated as annotation for enrichment analysis. Bottom: roteins correlating to ATRX across IDHmut tumors. Proteins annotated with telomerase-related terms color-coded (terms of top panel). Proteins linked to more than one term assigned color code of term with fewest proteins.

C) Survival association of chromosome 10 (left) and chromosome 7 (right) proteins regulated between IDHwt (n=11) and HGG-IDHmut-B (n=9). Select outlier proteins are colored based on the association of their transcripts with survival in the TCGA (The Cancer Genome Atlas) study. Top: Regulation. Bottom: Relationship between differential abundance and genomic position of proteins encoded on chromosome 10 (left) or chromosome 7 (right).

D) Survival association of chromosome arm 1p (left) and 19q (right) proteins regulated between codel (n=11) and non-codel IDHmut (n=10). Select outlier proteins are colored based on the association of their transcripts with survival in the TCGA (The Cancer Genome Atlas) study. Top: Regulation. Bottom: Relationship between differential abundance and genomic position of proteins encoded on chromosome arm 1p (left) or chromosome arm 19q (right).

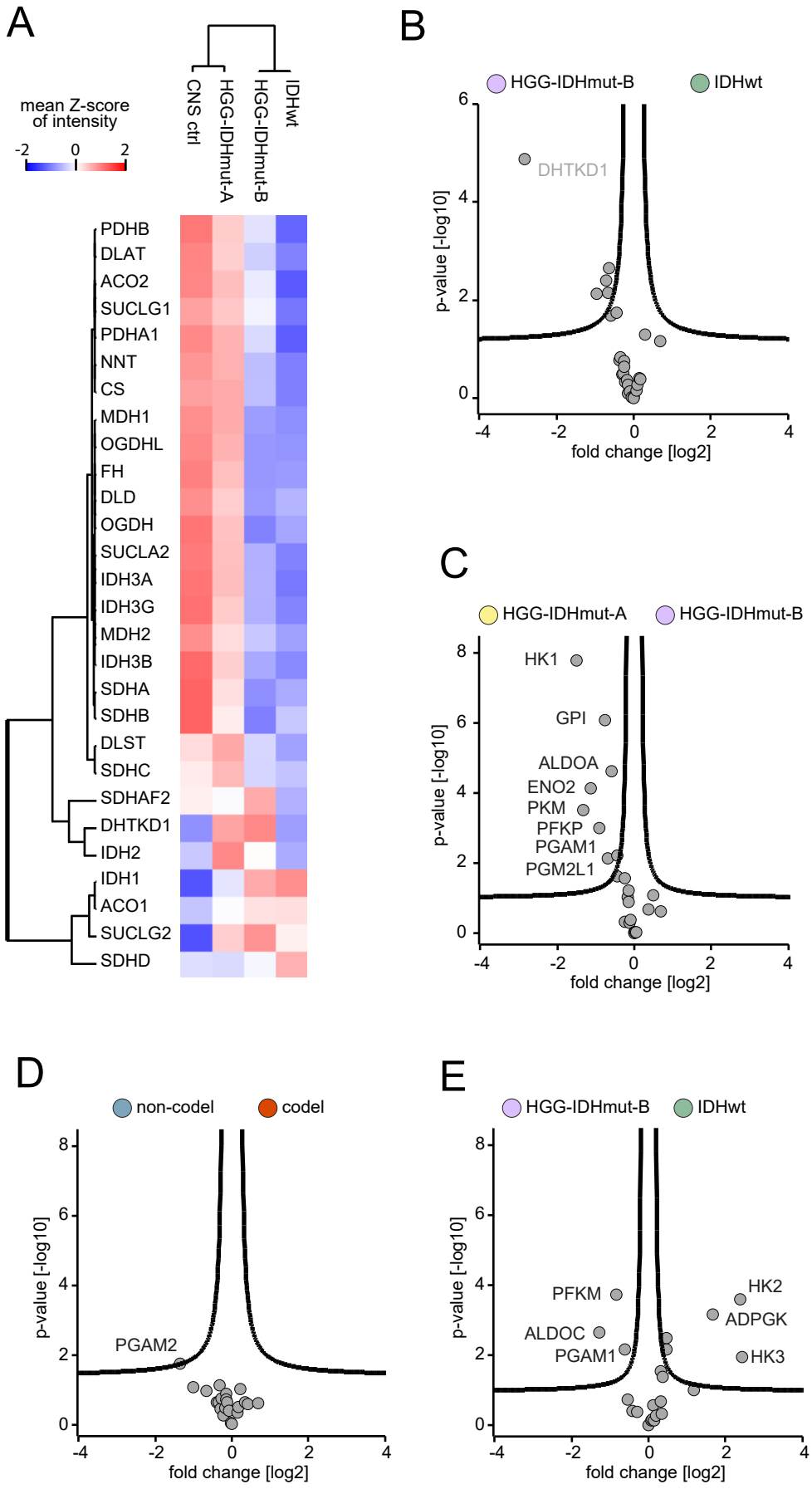
A
mean Z-score of intensity
-2
0
2
CNS ctrl
HGG-IDHmut-A
HGG-IDHmut-B
IDHwt
PDHB
DLAT
ACO2
SUCLG1
PDHA1
NNT
CS
MDH1
OGDHL
FH
DLD
OGDH
SUCLA2
IDH3A
IDH3G
MDH2
IDH3B
SDHA
SDHB
DLST
SDHC
SDHAF2
DHTKD1
IDH2
IDH1
ACO1
SUCLG2
SDHD
B
HGG-IDHmut-B
IDHwt
DHTKD1
p-value [-log10]
fold change [log2]
C
HGG-IDHmut-A
HGG-IDHmut-B
HK1
GPI
ALDOA
ENO2
PKM
PFKP
PGAM1
PGM2L1
p-value [-log10]
fold change [log2]
D
non-codel
codel
PGAM2
p-value [-log10]
fold change [log2]
E
HGG-IDHmut-B
IDHwt
PFKM
ALDOC
PGAM1
HK2
ADPGK
HK3
p-value [-log10]
fold change [log2]

Figure S4. Tricarboxylic acid cycle and glycolysis. Related to Figure 3.

A) Abundance of tricarboxylic acid cycle proteins across alternatively-defined entities of this study. Clustering associates the HGG-IDHmut-B sample group with IDHwt and HGG-IDHmut-A with ctrl CNS. Abundance as sample group mean of cross-sample Z-Scored intensity. Samples, n=10 (ctrl CNS), n=11 (IDHwt), n=11 (codel), n=10 (non-codel).

B) Regulation of tricarboxylic acid cycle proteins between IDHwt (n=11) and HGG-IDHmut-B (n=9).

C-E) Regulation of glycolysis proteins between HGG-IDHmut-B and HGG-IDHmut-A (C), codel and non-codel (D), and IDHwt and HGG-IDHmut-B (E). Samples, n=12 (HGG-IDHmut-A), n=9 (HGG-IDHmut-B), n=11 (IDHwt), n=11 (codel), n=10 (non-codel).

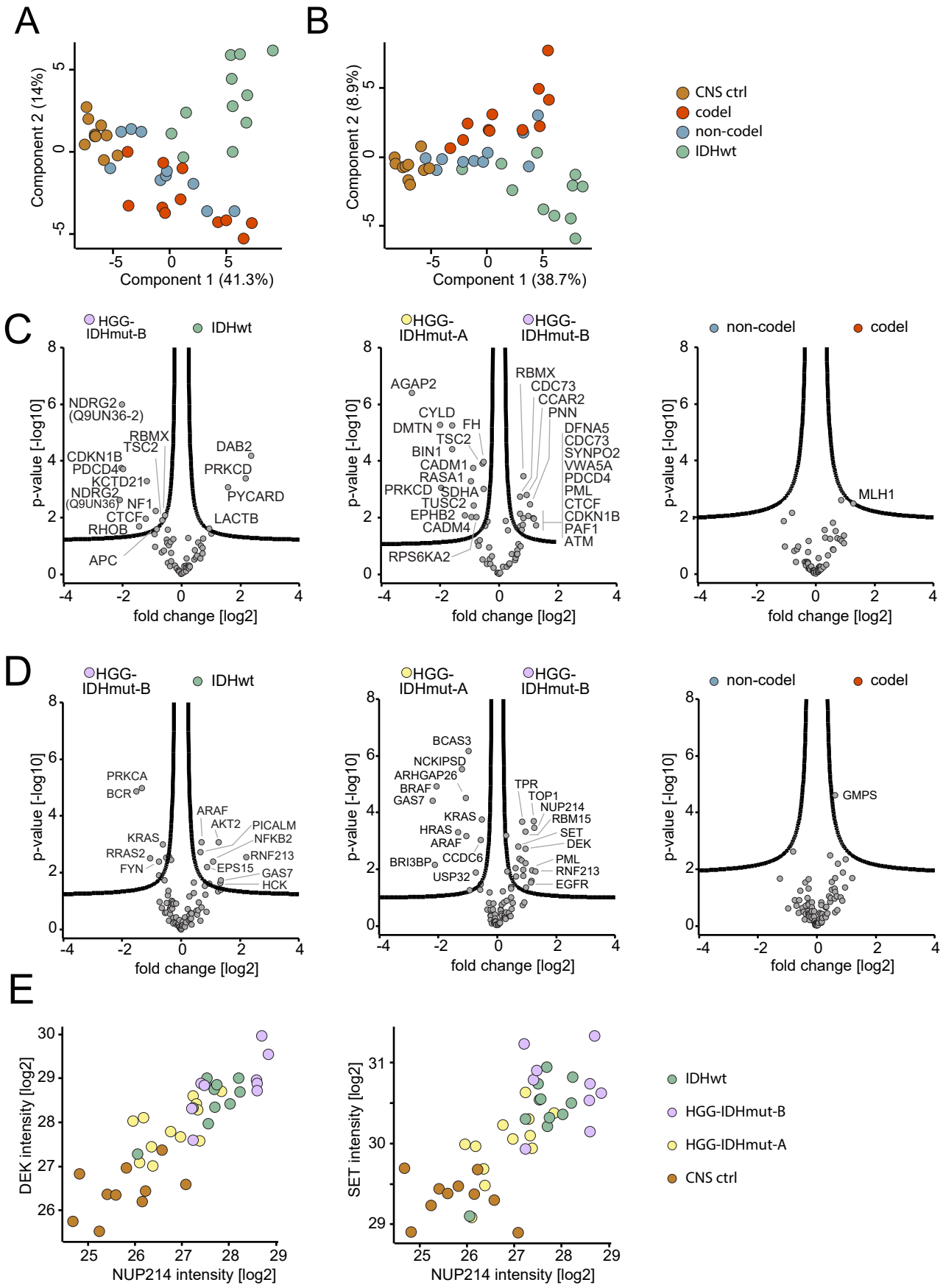
A
Component 2 (14%)
Component 1 (41.3%)
B
Component 2 (8.9%)
Component 1 (38.7%)
CNS ctrl
codel
non-codel
IDHwt
C
HGG-IDHmut-B
IDHwt
HGG-IDHmut-A
HGG-IDHmut-B
non-codel
codel
p-value [-log10]
fold change [log2]
NDRG2 (Q9UN36-2)
RBMX
TSC2
CDKN1B
PDCD4
KCTD21
NDRG2 (Q9UN36)
NF1
CTCF
RHOB
APC
DAB2
PRKCD
PYCARD
LACTB
AGAP2
CYLD
DMTN
FH
TSC2
BIN1
CADM1
RASA1
PRKCD
SDHA
TUSC2
EPHB2
CADM4
RPS6KA2
RBMX
CDC73
CCAR2
PNN
DFNA5
CDC73
SYNPO2
VWA5A
PDCD4
PML
CTCF
CDKN1B
PAF1
ATM
MLH1
D
HGG-IDHmut-B
IDHwt
HGG-IDHmut-A
HGG-IDHmut-B
non-codel
codel
p-value [-log10]
fold change [log2]
PRKCA
BCR
KRAS
RRAS2
FYN
ARAF
AKT2
PICALM
NFKB2
RNF213
EPS15
GAS7
HCK
BCAS3
NCKIPSD
ARHGAP26
BRAF
GAS7
KRAS
HRAS
ARAF
BRI3BP
CCDC6
USP32
TPR
TOP1
NUP214
RBM15
SET
DEK
PML
RNF213
EGFR
GMPS
E
DEK intensity [log2]
NUP214 intensity [log2]
SET intensity [log2]
NUP214 intensity [log2]
IDHwt
HGG-IDHmut-B
HGG-IDHmut-A
CNS ctrl

Figure S5. No separation of codel and non-codel entity in the tumor suppressor and proto-oncogene proteomes. Related to Figure 4.

A-B) Principal component analysis of UniProt Keyword-annotated tumor suppressor gene (A) and proto-oncogene (B) datasets. Samples, n=10 (ctrl CNS), n=11 (IDHwt), n=11 (codel), n=10 (non-codel).

C) Regulation of tumor suppressors between IDHwt and HGG-IDHmut-B (left), HGG-IDHmut-B and HGG-IDHmut-A (center), and codel and non-codel (right). Samples, n=10 (ctrl CNS), n=12 (HGG-IDHmut-A), n=9 (HGG-IDHmut-B), n=11 (IDHwt), n=11 (codel), n=10 (non-codel).

D) Regulation of oncoproteins between IDHwt and HGG-IDHmut-B (left), HGG-IDHmut-B and HGG-IDHmut-A (center), and codel and non-codel (right). Samples as in C.

E) Correlation of protein abundances of NUP214 and DEK (left), and NUP214 and SET (right) across samples. Pearson correlation coefficients r = 0.87 (left) and r = 0.76 (right). Samples as in C.

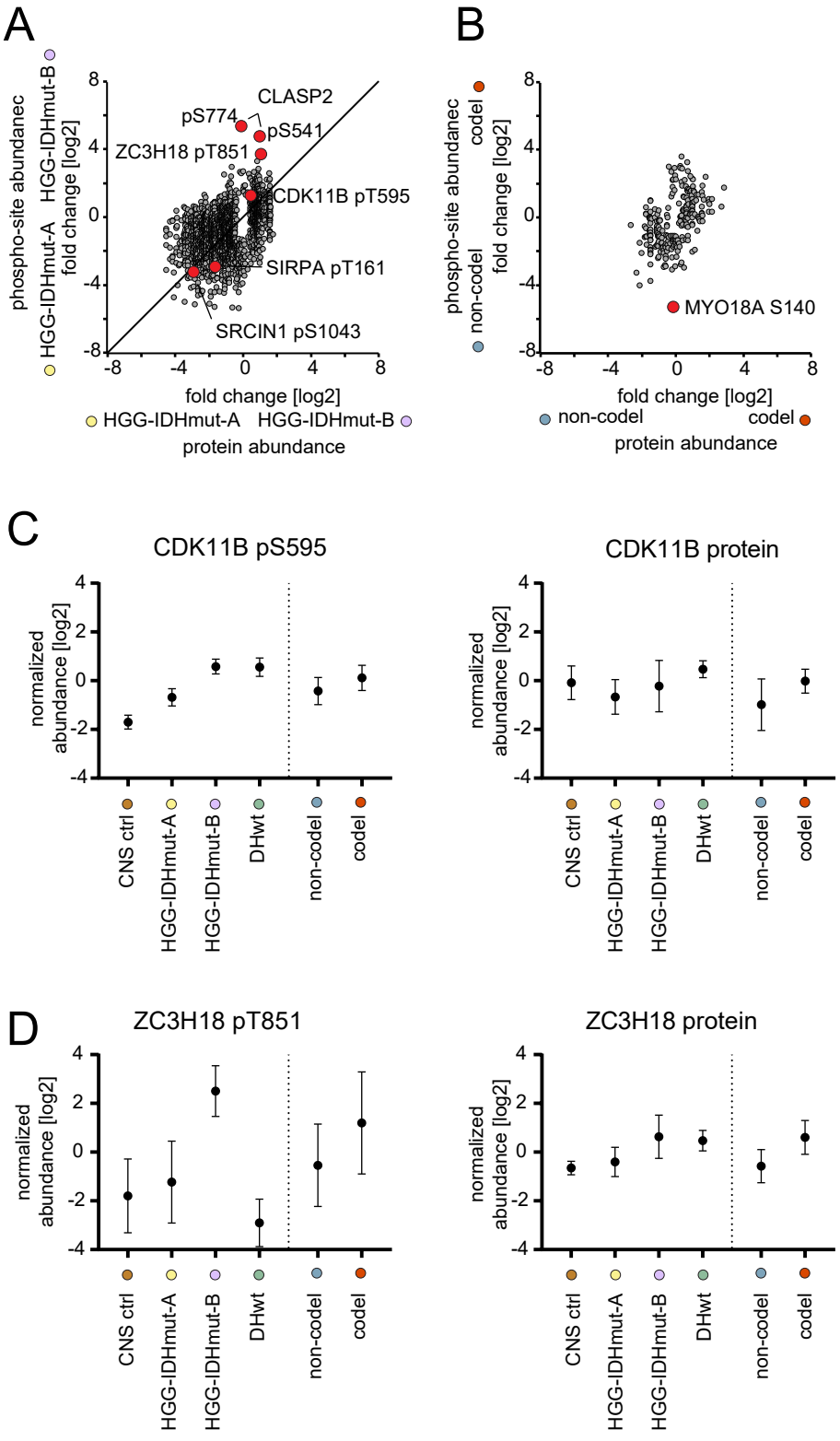
A
phospho-site abundanec
HGG-IDHmut-B
HGG-IDHmut-A
fold change [log2]
CLASP2
pS774
pS541
ZC3H18 pT851
CDK11B pT595
SIRPA pT161
SRCIN1 pS1043
fold change [log2]
HGG-IDHmut-A HGG-IDHmut-B
protein abundance
B
phospho-site abundanec
codel
non-codel
fold change [log2]
MYO18A S140
fold change [log2]
non-codel codel
protein abundance
C
CDK11B pS595
normalized abundance [log2]
CNS ctrl
HGG-IDHmut-A
HGG-IDHmut-B
DHwt
non-codel
codel
CDK11B protein
normalized abundance [log2]
CNS ctrl
HGG-IDHmut-A
HGG-IDHmut-B
DHwt
non-codel
codel
D
ZC3H18 pT851
normalized abundance [log2]
CNS ctrl
HGG-IDHmut-A
HGG-IDHmut-B
DHwt
non-codel
codel
ZC3H18 protein
normalized abundance [log2]
CNS ctrl
HGG-IDHmut-A
HGG-IDHmut-B
DHwt
non-codel
codel

Figure S6. Phosphosite dynamics in IDHmut glioma. Related to Figure 4.

A-B) Relationship of phosphosite abundance differences and protein abundance differences, each between HGG-IDHmut-B and HGG-IDHmut-A (A) and codel and non-codel (B). Outliers labelled in Fig. 4C also labelled here with gene name and phosphorylation site. Phosphorylation sites included if abundance difference in at least one dimension (phosphosite, protein) significant with q-value < 5% (A) or p-value < 0.05% (less stringent) (B). Diagonal line marks 1:1 relationship. Samples, n=12 (HGG-IDHmut-A), n=9 (HGG-IDHmut-B), n=11 (codel), n=10 (non-codel).

C-D) Abundance of CDK11B phosphorylation site pS595 (C) and ZC3H18 phosphorylation site pT851 (D) and protein abundances, respectively. Circles denote means and bars 95% confidence intervals of means. Samples, n=10 (ctrl CNS), n=12 (HGG-IDHmut-A), n=9 (HGG-IDHmut-B), n=11 (IDHwt), n=11 (codel), n=10 (non-codel).

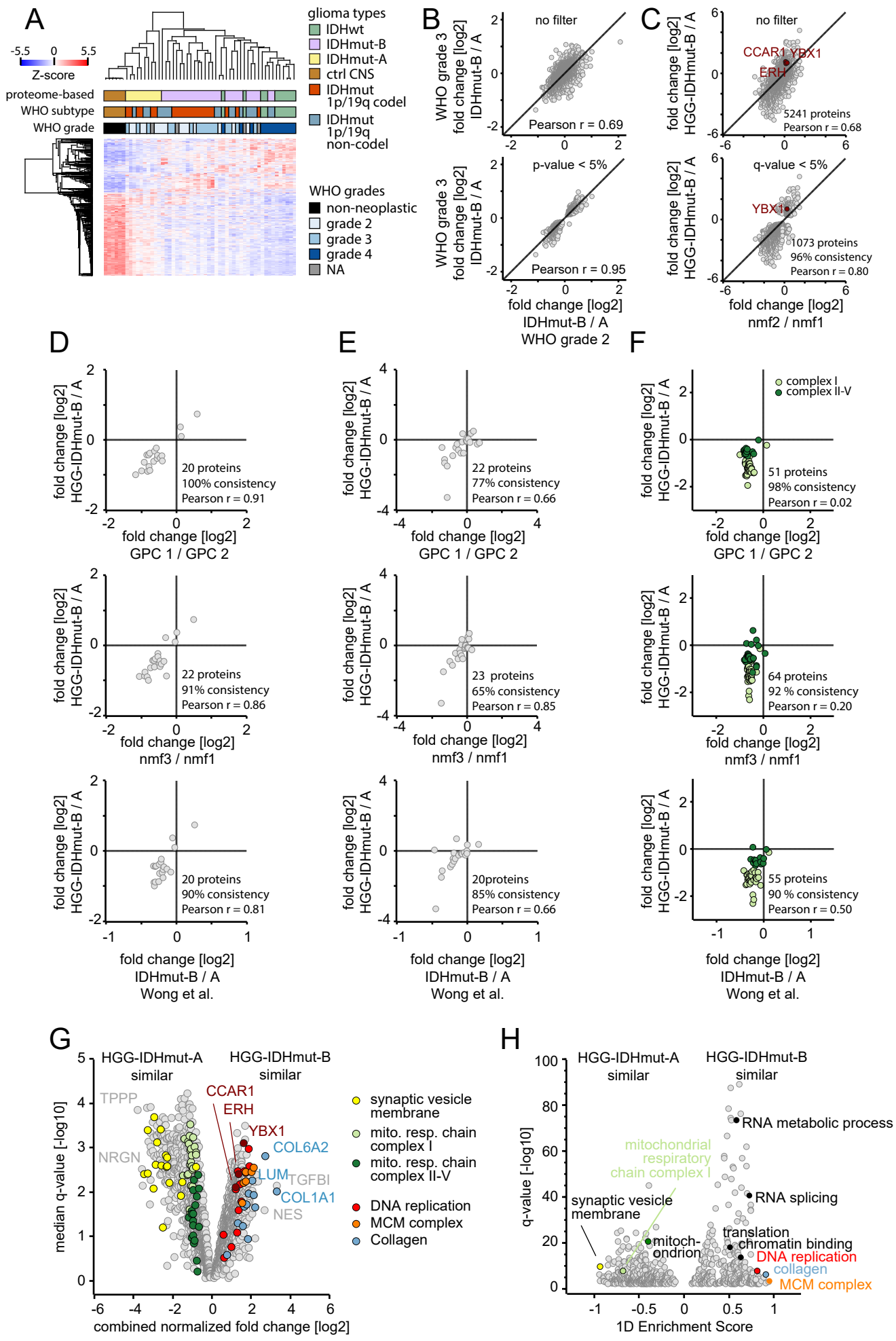
A
-5.5 0 5.5
Z-score
proteome-based
WHO subtype
WHO grade
glioma types
IDHwt
IDHmut-B
IDHmut-A
ctrl CNS
IDHmut 1p/19q codel
IDHmut 1p/19q non-codel
WHO grades
non-neoplastic
grade 2
grade 3
grade 4
NA
B
no filter
Pearson r = 0.69
p-value < 5%
Pearson r = 0.95
WHO grade 3 fold change [log2] IDHmut-B / A
fold change [log2] IDHmut-B / A WHO grade 2
C
no filter
CCAR1 YBX1
ERH
5241 proteins
Pearson r = 0.68
q-value < 5%
YBX1
1073 proteins
96% consistency
Pearson r = 0.80
fold change [log2] HGG-IDHmut-B / A
fold change [log2] nmf2 / nmf1
D
20 proteins
100% consistency
Pearson r = 0.91
22 proteins
91% consistency
Pearson r = 0.86
20 proteins
90% consistency
Pearson r = 0.81
fold change [log2] GPC 1 / GPC 2
fold change [log2] nmf3 / nmf1
fold change [log2] IDHmut-B / A Wong et al.
E
22 proteins
77% consistency
Pearson r = 0.66
23 proteins
65% consistency
Pearson r = 0.85
20proteins
85% consistency
Pearson r = 0.66
F
complex I
complex II-V
51 proteins
98% consistency
Pearson r = 0.02
64 proteins
92 % consistency
Pearson r = 0.20
55 proteins
90 % consistency
Pearson r = 0.50
G
HGG-IDHmut-A similar
HGG-IDHmut-B similar
TPPP
NRGN
CCAR1
ERH
YBX1
COL6A2
LUM
TGFBI
COL1A1
NES
median q-value [-log10]
combined normalized fold change [log2]
synaptic vesicle membrane
mito. resp. chain complex I
mito. resp. chain complex II-V
DNA replication
MCM complex
Collagen
H
HGG-IDHmut-A similar
HGG-IDHmut-B similar
RNA metabolic process
mitochondrial respiratory chain complex I
RNA splicing
synaptic vesicle membrane
translation
mitoch-ondrion
chromatin binding
DNA replication
collagen
MCM complex
q-value [-log10]
1D Enrichment Score

Figure S7. Integration of other proteomic glioma datasets. Related to Figure 5.

A) Identification of IDHmut-A and IDHmut-B in the Wong et al. dataset by Pearson coefficient-based hierarchical clustering of samples and ANOVA-significant (s0 = 2, q < 5%) proteins regulated by WHO-defined glioma subtype (IDHwt, IDHmut 1p/19 codel, IDHmut 1p/19q non-codel). Samples, n=6 (ctrl CNS), n=10 (IDHmut-A), n=28 (IDHmut-B), n=10 (IDHwt) and according to WHO classification n=21 (IDHmut 1p/19q-codeleted), n=17 (IDHmut non-codeleted, n=10 (IDHwt).

B) Comparison of fold changes between IDHmut-A and IDHmut-B in glioma samples in the Wong et al. dataset with WHO grade 2 (x axis, 6 IDHmut-A glioma, 9 IDHmut-B glioma) to those fold changes in glioma samples of WHO grade 3 (y axis, 3 IDHmut-A glioma, 13 IDHmut-B glioma) for all proteins (upper panel, 5897 proteins) and significantly regulated proteins (p < 5% in both comparisons, lower panel, 703 proteins). When filtering for significantly regulated proteins (p < 5%) in at least 1 of the two comparisons (within WHO 2, within WHO 3), 2050 proteins included and Pearson r = 0.81 (scatter plot not shown).

C) Comparison of fold changes between nmf2 ("mesenchymal-like", n=37) and nmf1 ("proneural-like, n=29) of the Wang et al./CPTAC dataset (x axis) and HGG-IDHmut-B (n=9) and HGG-IDHmut-A (n=12) in the dataset of this study (y axis) for all overlapping proteins (upper panel) and proteins significantly regulated (q < 5%) in both datasets.

D-F) Comparison of metabolic proteins across studies. Fold changes HGG-IDHmut-B (n=9) / HGG-IDHmut-A (n=12) (this study) compared to those of corresponding glioma subgroups GPC1 (n=26) / GPC2 (n=13) (Oh et al. dataset), nmf3 (n=25) / nmf1 (n=29) (Wang et al./CPTAC dataset), and IDHmut-B (n=28) / IDHmut-A (n=10) (Wong et al. dataset) for tricarboxylic acid cycle proteins (D), glycolysis proteins (E), and mitochondrial respiratory chain proteins (F).

G) Regulated proteins across four datasets in pseudo-Volcano plot. Proteins included were either consistenly enriched in HGG-IDHmut-B, nmf3, GPC1, IDHmut-B compared to HGG-IDHmut-A, nmf1, GPC2, IDHmut-A (dataset of this study, Wang/CPTAC et al., Oh et al., Wong et al.), respectively, or consistently inversely regulated. Sample numbers as in D-F. Protein fold changes normalized within each dataset after consistency filtering by division of mean (across proteins) absolute fold change separately for positive and negative fold changes. Subsequently, combined protein fold change (x axis) and q-value (y axis) calculated as median across the four studies.

H) Enrichment of functional protein annotation terms in the combined normalized fold change dimension of (G) by Perseus 1D Enrichment analysis. Terms displayed filtered for at least five member proteins and enrichment q-value of 1%.